JOURNAL OF MATERIALS SCIENCE 18 (1983) 2471–2483

Superplastic flow and failure at 773 K in the aluminium–calcium eutectic alloy

G. PIATTI
Materials Science Division, Ispra Establishment – Joint Research Centre, Commission of the European Communities, 21020 Ispra (Va), Italy

The superplastic behaviour of the hot rolled Al–Ca eutectic alloy (7.6 wt % Ca) was investigated at a temperature, $T = 773$ K, with strain rates varying from 2×10^{-5} to $4 \times 10^{-1}\,\text{sec}^{-1}$ and for a grain size of the order of 3 μm. The results showed that the stress strain rate behaviour could be divided into two distinct portions: (a) region II at intermediate and low strain rates ($\dot{\epsilon} \leqslant 4 \times 10^{-2}\,\text{sec}^{-1}$) where the strain rate sensitivity index, m, was $\geqslant 0.30$ (superplastic regime); (b) region III at higher strain rates ($\dot{\epsilon} > 4 \times 10^{-2}\,\text{sec}^{-1}$) where m was < 0.30 (conventional deformation regime). Elongations at fracture of greater than 300% were achieved on the region II of superplasticity (maximum value about 570%). There was experimental evidence in superplastic flow conditions of a grain boundary sliding process and dislocation activity within the aluminium matrix grains. The fracture depended on a void linkage mechanism which included on a microscopic scale the internal necking of the tiny ligaments already formed between the cavities.

1. Introduction

Extensive investigations concerning micrograin superplasticity have been carried out in recent years. On the one hand a satisfactory knowledge of the physical mechanisms operating during superplastic deformation has been obtained and on the other hand a capacity of very large deformations at low stresses has been discovered in modified materials or in new materials. Recently [1–3], superplastic behaviour characterized by a large elongation to fracture of many hundred per cent (1500% is the maximum value obtained to data) and a high strain rate sensitivity ($m \geqslant 0.3$) was achieved in the Al–Ca eutectic after suitable preparation (chill casting and heavy hot working) which produced a fine morphology (aluminium matrix grain size $\leqslant 10\,\mu$m) stabilized by the presence of a large volume (31%) [2] of Al_4Ca second phase. Any coarsening of the grain would in fact lead to complete loss of the large deformation capability. Superplasticity was exhibited only above temperature $T \cong 673$ K and over an intermediate strain range (10^{-4} to $10^{-2}\,\text{sec}^{-1}$) [2]. The superplastic behaviour of the hot rolled Al–Ca eutectic was confirmed by successful production of deep hollow and walled complex components [4]. Finally, it was shown that in service the Al–Ca alloy possesses moderate strength [1–6] but quite good corrosion resistance [3, 7] making it suitable for complex and unloading bearing structures [4].

The Al–Ca eutectic reaction occurs at a nominal composition of 7.6 wt % (5.3 at %) Ca and at a temperature of 890 K [8]. The phase in equilibrium with aluminium is the body centred tetragonal Al_4Ca [9]. This intermetallic is caused by a peritectic reaction at 970 K [8]; it is harder (Vickers hardness 2000 to 2600 MPa) [8] than pure aluminium and it is brittle up to 573 K whereas it is ductile above 673 K [5, 6]. The solubility of calcium is very low ($< 0.05\%$ at 873 K) [6]. The eutectic morphology was observed over a broad range of composition (coupled growth zone) on both sides of the eutectic composition between 6.5 and 8.5 wt % Ca [9, 10].

However, despite the number of studies listed above, there has been until now no precise assessment of the strain rate sensitivity, m, in the Al–Ca alloy, the most important parameter which regulates the superplastic flow. Moreover, good

0022–2461/83 $03.00 + .12

understanding of the dependence of strain rate on applied stress, on ductility and on microstructure could have useful implications for superplastic forming. For this reason the author performed a series of mechanical tests (uniaxial tension) with a large variety of strain rates at one temperature (chosen on the range of Al–Ca alloy optimal superplastic conditions resulting from a previous work [2]) on several samples of a hot rolled Al–Ca alloy prepared on a laboratory scale. Topological and microstructural observations with optical and electron optical techniques were also carried out on some specimens before and after superplastic deformation. The results obtained are presented and discussed in the present work.

2. Experimental details

2.1. Materials preparation

A master alloy of about 30 wt% Ca was first prepared by induction melting of the pure components (Al 99.995% and Ca 99.95% purity) in an amorphous carbon crucible under a positive pressure of argon. One ingot of eutectic composition was then prepared by remelting and diluting the master alloy with a suitable amount of aluminium and chill casting. The ingot (see the microstructure in Fig. 1) was cleaned to remove the surface defects and was first extruded ($T \sim 773$ K) into a 55 mm x 5 mm plate and then hot rolled ($T \sim 673$ K) into 1 mm thick sheet with the effect of breaking up the lamellar structure and of obtaining a microduplex structure constituted of an intimate mixture of aluminium (matrix) and Al_4Ca (second phase particles) (Fig. 2). No annealing was used after the double working procedure (extrusion plus rolling) because the dynamic recrystallization which occurred during the hot deformation was sufficient to produce the equiaxed fine grain structure required for extensive superplasticity. A chemical analysis of the final product was 7.7 wt% Ca. Impurities were 50 ppm Fe, 50 ppm Si and 10 ppm Mg. The small compositional difference from the nominal 7.6 wt% Ca did not affect the superplastic behaviour. Flat specimens of 8 mm gauge length, 2 mm gauge width and 1 mm thickness were stamped from the sheets with their tensile axis parallel to the rolling direction.

2.2. Testing

Tensile tests were conducted on an Instron electromechanical machine (capable of various crosshead

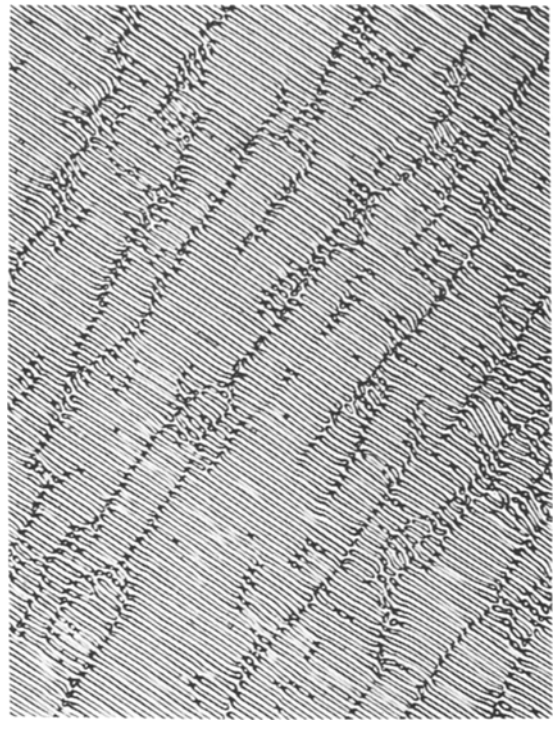

Figure 1 Optical micrograph of cast Al–Ca eutectic alloy. Both phases form lamellae (white aluminium, grey Al_4Ca) aligned parallel to each other (×1000).

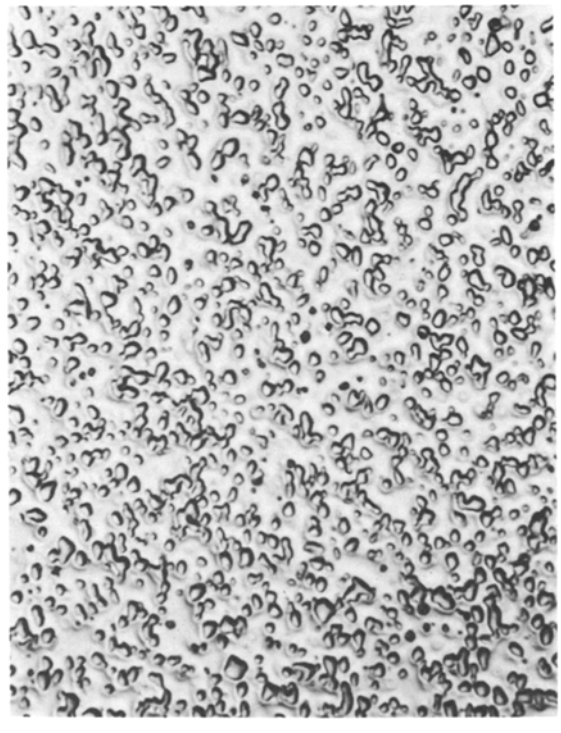

Figure 2. Optical micrograph of transverse section of hot rolled Al–Ca eutectic alloy. The aluminium matrix grains are not visible despite overetching (×1000).

speeds) at a temperature, 773 K, over a wide initial strain rate range (4.16×10^{-5} to $4.16 \times 10^{-1}\,sec^{-1}$). All specimens used were pulled to fracture at a single constant rate of crosshead displacement. This means an approximate (not true) constant rate because there is a continuously decreasing effective strain velocity. An argon atmosphere furnace controlled to ± 2 K was employed. After loading the tensile specimen into the furnace, a delay of 15 min was necessary to ensure that a uniform test temperature was achieved. The experimental load–extension diagrams obtained from the tensile tests were stored point-wise in an electronic computer and then processed to obtain the true stresses, true strain and the true strain rates assuming constant volume of the specimen during tensile deformation. In fact, although engineering stress, strain and strain rate values are often used to characterize the mechanical behaviour, it is preferable, in the case of superplastic materials, to use the true values of the above parameters because of the large strain rate dependence and of the large elongations exhibited. The strain rate sensitivity index ($m = \delta \log\sigma / \delta \log\dot{\epsilon}$, where σ is the true flow stress at a prefixed strain level and $\dot{\epsilon}$ the true strain rate) was determined from the slope of the $\log\sigma$ against $\log\dot{\epsilon}$ plot.

The virgin material and the deformed tensile specimen were transversally and longitudinally sectioned and samples for metallographic examination were polished and etched in a solution (5 vol% perchloric acid plus 20 vol% ether in ethanol) which revealed the second phase particles in strong contrast. On the other hand, the aluminium grain size was not distinguishable due to the difficulty in etching the boundaries in the Al–Ca microduplex materials [2, 6]. As a result the grain size, d, of the Al_4Ca second phase was used instead of the aluminium matrix grain size, L. This assumption is justified by the fact that in the hot rolled Al–Al_4Ca eutectic there is a linear relationship between the aluminium mean grain size $\bar{L}$ and the Al_4Ca mean particle size, $\bar{d}$, as shown in an extensive investigation on the Al–Ca alloys by Jaquet and Warlimont [6]:

$$\bar{L} \cong 1.13\bar{d}. \tag{1}$$

The $\bar{d}$ values were obtained by employing the known formula

$$\bar{d} = \frac{3}{2}\frac{F}{N_L} \tag{2}$$

where F is the second phase fraction ($F = 0.31$) [2] and N_L is the number of the second phase particles intercepted per unit length by lines of equal length superimposed on several light and scanning electron microscopy (SEM) images. For the determination of one mean grain size 500 to 1500 particles were analysed. The effective grain diameter was obtained from the relation [6]:

$$d = (\bar{d}_1 \times \bar{d}_2 \times \bar{d}_3)^{1/3} \tag{3}$$

where d_1, d_2 and d_3 are the grain sizes determined, respectively, in the rolling, transverse and short direction. Moreover, taking into account that the grain size distribution for alloys obtained by linear intercept is generally represented by a log normal function, a computer analysis by a curve fitting program was performed.

A transmission electron microscopy (TEM) examination was also carried out in the virgin material and on some specimens of which superplastically deformed, using different precautions in order to ensure that no damage was introduced during the thin foil preparation. Several plates were obtained by spark machining from the specimens and thinned by electropolishing (25 V) at 333 K on a solution of 33% nitric acid on methanol. The topological and morphological analyses were completed with a careful examination on a scanning electron microscope of the surface and fracture areas of some deformed specimens.

3. Results and discussion

3.1. Stress–strain behaviour

Fig. 3 shows a representative set of the true stress (σ)–true strain (ϵ) curves calculated from the Instron load against elongation results obtained at different crosshead velocities. At low and moderate initial strain rates ($\dot{\epsilon}_0 \leqslant 4.16 \times 10^{-2}\,sec^{-1}$) there is an immediate strain hardening which is followed by a steady-state flow in which the stress is practically strain independent. The delay necessary to attain the steady flow increases with increasing strain rate. At higher initial strain rate ($\dot{\epsilon}_0 > 4.16 \times 10^{-2}\,sec^{-1}$) some strain softening follows the strain hardening and the mechanical behaviour tends to be more conventional. There is a strain dependence of the flow stress in the early parts of deformation ($\epsilon \leqslant 0.5$) which can influence the stress (σ)–strain rate ($\dot{\epsilon}$) behaviour and also the parameter of the constitutive relations for superplasticity as discussed in the next section.

The strain hardening can be attributed to the

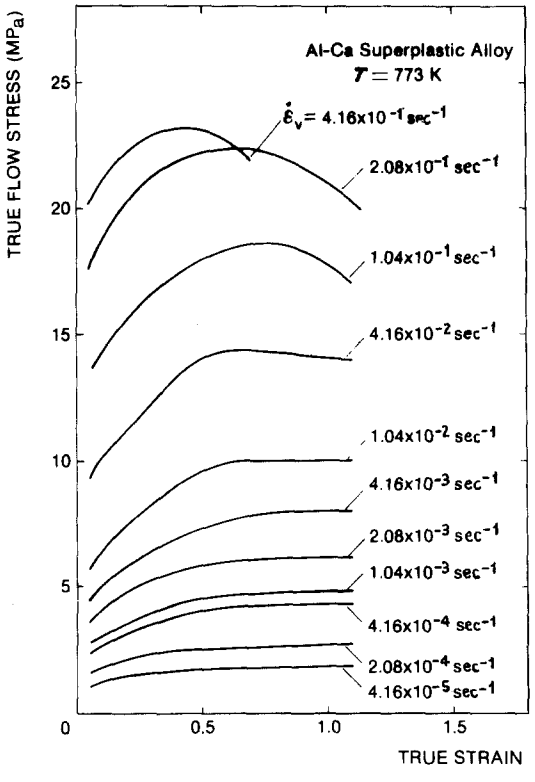

Figure 3. Representative true stress–true strain curves at a variety of strain rates.

grain coarsening and not to the increase of the structure defects. There are similar cases in the literature: Pb–Sn eutectic [11], where the connection between strain hardening and grain coarsening was clearly established, and Al–Cu eutectic [12] in which Watts and Stowell found that the flow stress increased with strain and ascribed this feature to strain enhanced grain growth. The concurrent grain coarsening during initial deformation is clearly evident in this alloy (Section 3.4). The softening is probably due to the removal or destruction of directional defects produced by prior casting and rolling of the material, as previously suggested by Suery and Baudelet [13] for similar situations as in the case of 60/40 brass.

3.2. Stress–strain rate relationship

The flow stress is a strong function of the strain rate as shown in Fig. 4 where the true stress (σ) measured at various strain levels (true strain $\epsilon = 0.002, 0.10, 0.18$ and 0.69) is plotted logarithmically against the true strain rate ($\dot{\epsilon}$). Every data point is the mean of two experimental values. Although alternative relationships exist, the superplastic behaviour in Fig. 4 is generally described in the literature (see extensive reviews [14, 15]), by the empirical equation:

$$\sigma = K\dot{\epsilon}^m \qquad (4)$$

where K is a constant for a given temperature and material grain size and m, strain rate sensitivity, represents the slope of the logarithmic plot. The Equation 4 means that the flow stress is a unique function of the strain rate and that the influence of strain can be neglected. Many results reported in the literature [14, 15] seem to support this statement. However, it can be seen from Fig. 4 that the slope of the log stress–log strain rate curves change with increasing strain level. At very low strain ($\epsilon = 0.002$) the sigmoidal or S-shape

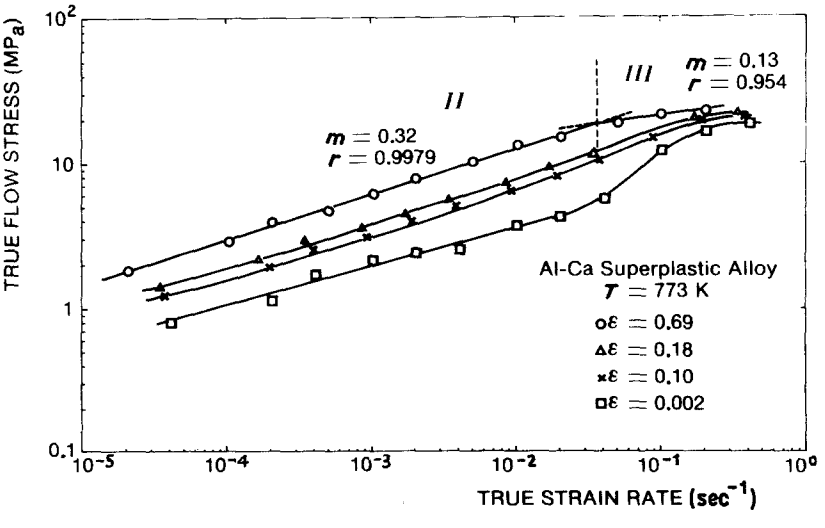

Figure 4. Log true stress–true strain rate for various true strains. The conventional division into region II (slope $m = 0.32$) and region III (slope $m = 0.13$) are indicated for the upper curve ($\epsilon = 0.69$). Concerning the other curves the m_{max} values are, respectively, 0.75 ($\epsilon = 0.002$), 0.42 ($\epsilon = 0.10$) and 0.38 ($\epsilon = 0.18$).

characteristics of several superplastic materials (previously reported for Al–Al_4Ca hot rolled eutectic in similar testing conditions [2]) is obvious. The maximum slope obtained is 0.75. On the other hand, at greater strain level ($\epsilon \geqslant 0.10$) the $\log\sigma$–$\log\dot{\epsilon}$ curve alters with increasing strain and tends to approach a straight line. The m maximum value decreases with increasing strain before the value $\epsilon = 0.69$ is reached. Beyond this point strain independent behaviour is observed because the steady-state flow is attained and m becomes independent of strain. A first conclusion from Fig. 4 is that an appropriate strain value must be chosen in computation of m in Equation 1. In other words, one must obtain a strain rate sensitivity parameter, m, representing stable microstructure. This requirement of comparable microstructural conditions between experiment and theory has been clearly shown in recent works by other authors [13, 16, 17]. The variation of m with strain determined from Fig. 4, is reported in Fig. 5. This variation could have important implications on formability testing and process of components.

A regression analysis applied to data (Fig. 4) taking into account $\epsilon = 0.69$ (steady flow stress conditions) gives, for the strain rates $\dot{\epsilon} \leqslant 4.10^{-2}$ sec^{-1}, a straight line with a correlation coefficient, r, better than 0.997 and with a slope $m = 0.32$ (conventionally region II), whereas for $\dot{\epsilon} > 4.10^{-2}$ sec^{-1} a straight line with $r = 0.954$ and a slope $m = 0.13$ is obtained (conventionally region III). In the region II (high strain rate sensitivity) superplasticity occurs. Region III (low strain rate sensitivity) is characterized conventionally by plasticity. The results then show no evidence of region I. It could be remarked that the absence in the superplastic Al–Ca alloy at low strain rates of the region I, could be due to the limited range of crosshead velocities used in the experiment. However, this hypothesis is not to be considered because the lowest true strain rate value reached in this work ($\sim 2 \times 10^{-5}$ sec^{-1}) is of the same order as the lowest strain rates (tensile tests) values reported in the literature [14, 15] concerning other superplastic systems investigated.

Although most of the superplasticity data show a sigmoidal or S relation between the log stress and log strain rate, there are also a number of examples where there is no conventional region I. Rai and Grant [18] found in the hot worked Al–Cu eutectic alloy a superplastic behaviour characterized by a strong stress dependence on strain and by a shape of log stress–log strain rate curve depending on strain at each crosshead speed (S-shape for strain less than $\epsilon = 0.05$ and linear for strains greater than about $\epsilon = 0.14$). Recently Lam *et al.* [19] have investigated the Pb–Sn eutectic alloy and found that the relationship between the stress and strain rate can be divided in two distinct regions if the data are taken after about $\epsilon = 0.5$. An obvious similarity then exists between the mentioned results [18, 19] and the present data: when the minimum strain required

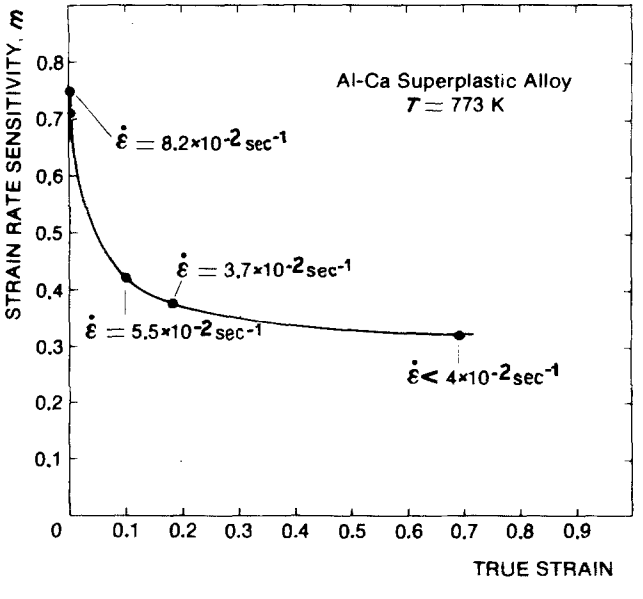

Figure 5. Strain dependence of the strain rate sensitivity, m, at 773 K over a strain rate range of 10^{-4} to 10^{-1} sec^{-1}.

for a valid data collection is attained, the logσ–log$\dot{\varepsilon}$ the curves become straight lines and the apparent shape disappears.

Finally, the present data appear not to support the existence of a threshold stress below which deformation does not appear to occur. However, even if a very small threshold stress could exist, it would not affect the logσ–log$\dot{\varepsilon}$ curve in the strain rate range covered by the present work.

3.3. Dependence of elongation on strain rate

The total elongation (i.e. the elongation at rupture) values are characterized by a large scatter, generally observed in superplastic materials, which makes it difficult to delineate the ductility trend against strain rate [14, 15]. Total elongations to failure of greater than 300% were achieved in the region II of superplasticity whereas in the region III ductility values drop below 200%. In a first approximation the elongation continues to increase slowly to the lowest strain rate ($\dot{\varepsilon}_0 = 4.16 \times 10^{-4}$ sec^{-1}) at which the total elongation was measured. A maximum value about 570% was obtained. This behaviour seems to be in agreement with the data on Al–Cu eutectic [18] previously mentioned, but not with other data reported in the literature [14, 15], which generally present a peak elongation. Moreover, as in the case of the Al–Cu alloy [18] the ductility appears not to be related to the m values. Woodford [20] has collected in a graph the total elongation percentages as a function of the m value for a wide range of materials (creep and superplastic tests). From the mentioned graph [20] we should have, considering $m = 0.32$, a total elongation of about 250%. This value does not fit the maximum ductility value (about 570%) obtained.

Ductility measurements are a reliable indicator of superplastic potential. As such it must be reminded that the present data do not show the maximum elongation available from the Al–Ca alloy because our data refer only to the temperature, 773 K. Generally in superplastic materials, the maximum ductility obtainable in the region II increases with increasing temperature and, as the testing temperature is increased, the maximum ductility occurs at a higher initial rate [14, 15]. Moreover, a high ratio initial specimen diameter–original gauge length leads to much higher elongation values [14, 15]. In fact, Grimes *et al.* [3] by using a test piece 12.5 mm gauge length by 6.25 mm gauge width by sheet thickness were able to obtain elongations at fracture of 1500%, by tensile test at 823 K (initial strain rate $\dot{\varepsilon}_v = 6.10^{-2}\,sec^{-1}$). It is then obvious that the present test temperature at 773 K is 50 K lower than the optimum for ductility.

3.4. Microstructure

The initial microstructure, shown at different magnifications in Fig. 2 and in Fig. 6, respectively, presents a random dispersion throughout the aluminium matrix of fine particles not very regular in shape but approximately equiaxed. The particles were identified by X-ray diffraction analysis as being intermetallic Al_4Ca, as envisaged in the Al–Ca diagram [8]. No particle size banding, usually present in two-phase hot rolled material, was observed. The average Al_4Ca grain size was assessed by quantitative metallography at 2 to 3 μm. More exactly the mean grain sizes determined on the different plate sections were: $\bar{d}_1 = 2.40\,\mu m$, $\bar{d}_2 = 2.18$ and $\bar{d}_3 = 2.39\,\mu m$, and final result following Equation 3 was 2.32 μm.

Taking into account Equation 1, the mean aluminium matrix grain size yields $\bar{L} = 2.32 \times 1.13 = 3.02\,\mu m$. The particle size distribution (Fig. 7) was revealed to be a log normal type and regular in the sense that it is not bimodal. The latter is quite common in materials for high temperature, superplastic alloys including [21]. The lack of banding and of irregular size distribution is due to the double hot working procedure (extension plus rolling), adopted for the fabrication of the alloy, which leads to a more homogeneous final product.

Electron microscopy (TEM analysis) permitted the observation of the matrix grains (not visible by light microscopy). Fig. 8 shows the initial microstructure which consists of an agregate of essentially equiaxed aluminium grains. The dislocations are arranged in a network of low angle boundaries. The previous observations [6] that the micromorphology of the hot rolled Al–Ca eutectic can be classified as strongly recovered, is fully borne out. The Al_4Ca particles density appears to be low because some of the particles have leached out during the electropolishing due to the difficulty in preparing samples for transmission electron microscopy of Al_4Ca eutectic alloy, as previously observed [6].

Internal changes produced during deformation were revealed. Limited particle coarsening of the

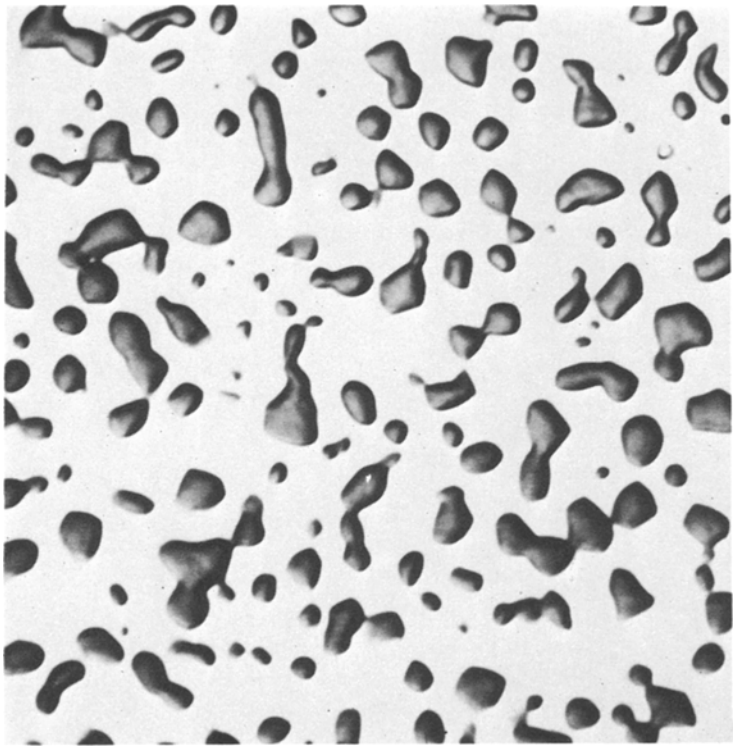

Figure 6. Optical micrograph of transverse section of the hot rolled Al–Ca eutectic alloy showing the particle shape and distribution (× 2040).

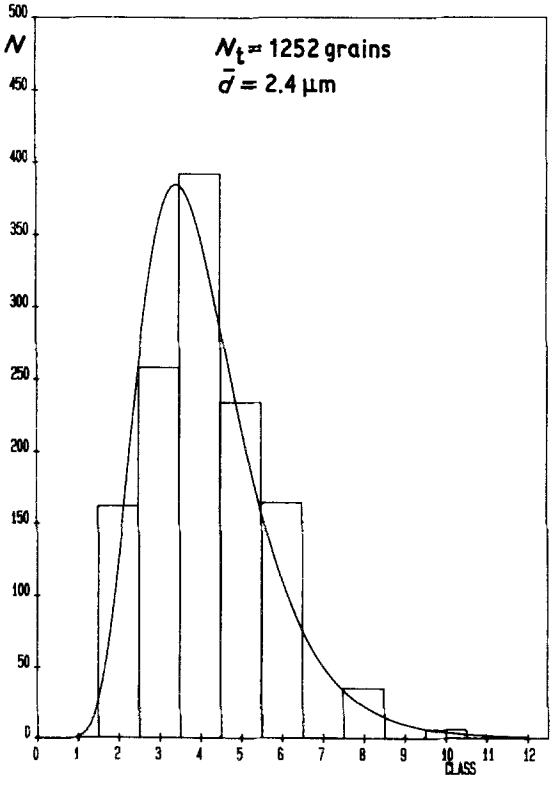

Figure 7. An example of distribution of the intercept diameter of the Al_4Ca particles. N is the number of the particles belowing to a single class, whereas N_t is the total number.

order of 60% after about 500% elongation was observed. This small amount of particle grain growth is typical of superplastic two-phase materials [14, 15]. However, there was considerable modification of the shape and distribution of the intermetallic Al_4Ca during deformation. As in the case of other superplastic aluminium eutectic alloys, Al–Cu [12] and Al–Pd [22], continuous breakdown and impingement of the second phase particles occurred. These microstructural changes, according to Watts and Stowell [12], can be understood in terms of sliding and diffusion-controlled shape changes associated with grain boundaries within the intermetallic phase. The grain size measurements performed in different zones of a deformed sample (elongation at rupture about 500% at an initial strain rate $\dot{\epsilon}_0 = 4.16 \times 10^{-3}\,sec^{-1}$) showed that the Al_4Ca grain coarsening is strain induced.

The TEM analysis, performed on some samples deformed in region II at an intermediate initial strain rate ($\dot{\epsilon}_0 = 4.16 \times 10^{-3}\,sec^{-1}$), showed that the microstructure remains equiaxed after many hundred per cent of superplastic deformation (Fig. 9). This behaviour is typical of the superplastic materials [14, 15] and is in strong contrast to conventional plastic deformation when a marked grain elongation is produced by a large

Figure 8. Transmission electron micrograph of Al–Ca alloy (initial state, i.e. after hot rolling). Note the presence of subgrain boundaries as well as high angle grain boundaries (×17 000).

extension. Grain coarsening occurs which can be seen from the comparison of Fig. 9 with Fig. 8, showing the microstructure of the virgin material. Interphase boundaries become curves (the less mobile Al_4Ca particles were spheroidized) whereas grain boundaries retaining their original configuration are straight. The dislocation tendency toward network and sub-boundary tends to disappear. In some grains a process of dislocation pile-ups is clearly visible with very fine impurity particles. Other grains are dislocation-free, but this fact does not necessarily mean that there is no intragranular slip during superplastic deformation but only that there are no obstacles to dislocation motion within the grain, as previously observed by several authors [14]. Then the TEM analysis in region II suggests dislocation motion within the aluminium matrix grains. Observations have not been performed in region III, but the stress exponent $n = 1/m = 7.69$ suggests the occurrence of a dislocation creep process such as dislocation climb.

As concerning the external aspect of the deformed samples (Fig. 10), considerable surface roughness was revealed by SEM analysis (see also Fig. 14). Moreover, a new surface has been created indicating that grains were moving out of the surface. These important features have also been reported by other authors and it can be attributed to grain boundary sliding processes.

3.5. Cavitation and failure

The specimens deformed in region III showed the conventional ductile rupture characterized by external necking, whereas the tensile deformation in superplastic conditions ($\dot{\epsilon} = 2 \times 10^{-5}$ to $4 \times 10^{-2}\,sec^{-1}$) terminate by intrinsic plastic failure. In fact, tensile specimens deformed in region II showed reductions in area near to 100% to fracture and without a significant external necking.

Figure 9. Transmission electron micrograph of the Al–Ca alloy after superplastic elongation of the order of 400% in region II ($\dot{\epsilon}_0 = 4.16 \times 10^{-3}\ sec^{-1}$). Dislocation pile-ups can be clearly seen (× 13 600).

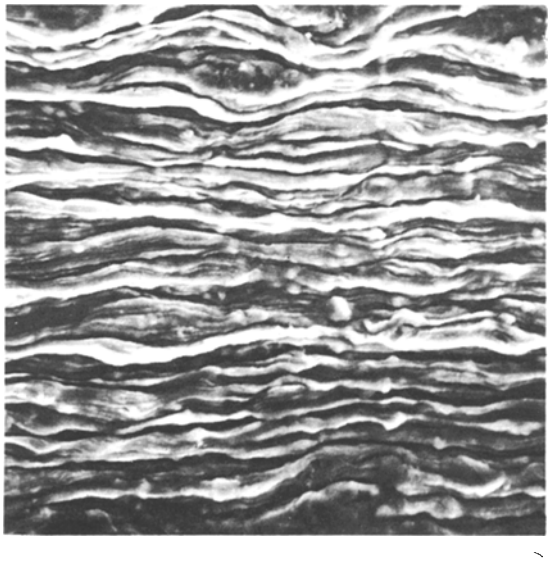

Figure 10. Surface appearance (scanning electron micrograph) of a specimen deformed about 400% of the superplastic Al–Ca alloy (× 700).

A limited cavitation was observed, by metallographic and SEM analysis, which seems to be compatible with large elongation as, for instance, in the highly superplastic alloy Zn–22 Al [23]. Cavities are nucleated at the intermetallic particles (preferentially larger ones) and growth occurs along the particle–matrix boundary (Fig. 11). The cavity formation is due, according to Livesey and Ridley [11], to difficulties in accommodation by diffusion or by dislocation motion over the relatively large interfacial area between particles and matrix. In fact, one should recall that in the case of the hot rolled Al–Ca the boundary of the aluminium grain is composed of 60% of Al–Al_4Ca interphase boundary [6].

Another factor which tends to promote void nucleation in two phase superplastic materials is the hardness of the second phase [11]. In other words, the degree of covalent or ionic bonding existing on the Al_4Ca intermetallic compounds could influence the level of cavitation.

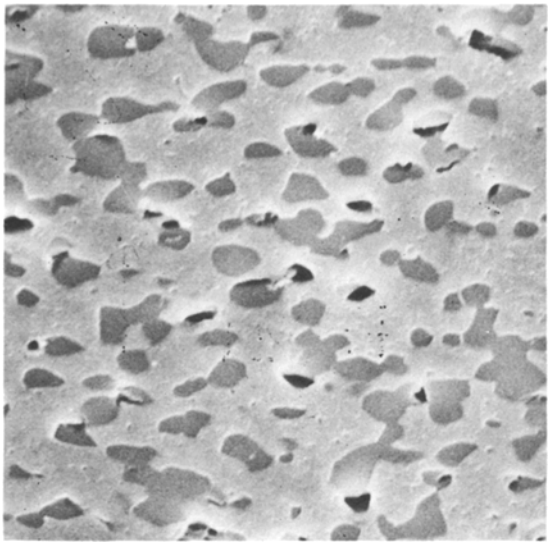

Figure 11. Scanning electron micrograph of longitudinal section of a sample (gauge length) of Al–Ca alloy after superplastic deformation (X 2000).

Cavitation seems dependent on strain rate in the sense that cavitation increases in magnitude as the initial strain rate is decreased. On the other hand, in the previously mentioned superplastic system [23], there is a clear rate dependence. Occasionally, internal cracks in Al_4Ca particles were observed, but these were produced by prior heavy hot rolling of the alloy. The situation is different for Al–Ca samples deformed at room temperature [6], where premature fracture of the Al_4Ca particles made a significant contribution to the nucleation and growth of the cavities.

The final stage of cavitation has been studied by SEM analysis. Figs. 12 to 14 show fracture areas of samples deformed in different conditions of initial strain rate ($\dot{\epsilon}_0 = 4.16 \times 10^{-4}$, 4.16×10^{-3} and $4.16 \times 10^{-2}\,sec^{-1}$). An array of tiny ligaments between the cavities is visible at the fine point of fracture (Figs. 12 and 13). The finer ($d \sim 0.5\,\mu m$) Al_4Ca particles seem not to be separated from the matrix. However, when the strain rate conditions ($\dot{\epsilon}_0 = 4.16 \times 10^{-2}\,sec^{-1}$) approach the conventional deformation regime in region III, there is no evidence of tiny ligaments (Fig. 14) but a significant cavitation always appears.

Failure of superplastic alloys can be classified into two types [15, 24]:

Figure 12. Scanning electron micrograph showing the cavitation at the tip fracture in an Al–Ca alloy specimen tested at an initial strain rate of $4.16 \times 10^{-4}\,sec^{-1}$ (region II) (×1360).

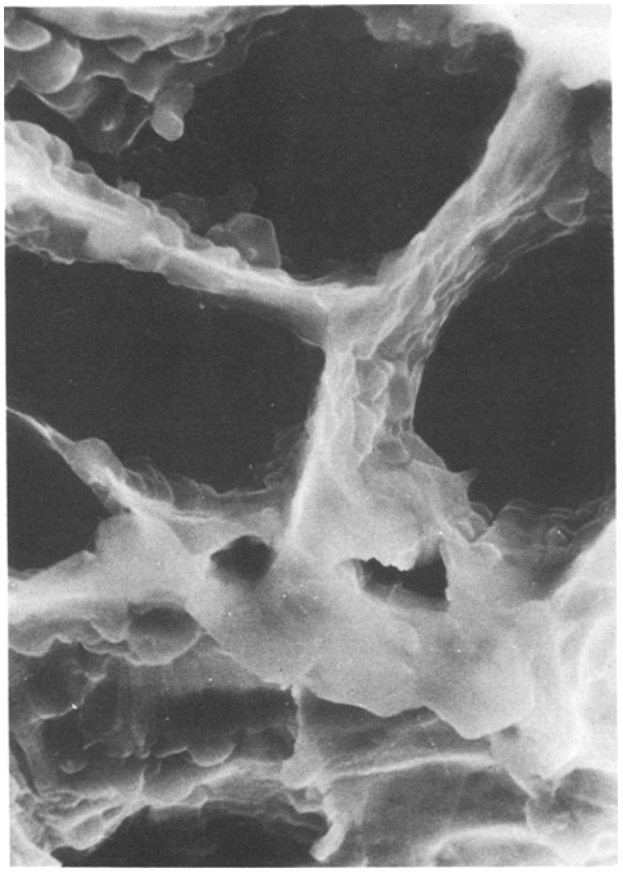

Figure 13. Scanning electron micrograph showing the cavitation at the tip fracture in an Al–Ca alloy specimen tested at an initial strain rate of $4.16 \times 10^{-3}\,sec^{-1}$ (region II) (×1700).

(i) intrinsic plastic failure determined by the necking characteristics of the materials and where the specimen pulls down to a very small point of fracture;

(ii) quasi-brittle failure where fracture takes place due to the internal necking. It is macroscopically planar when observed at low magnification.

The former occurs in the superplastic alloys which present little cavitation phenomena such as Zn–Al alloy [23], whereas the latter is character-

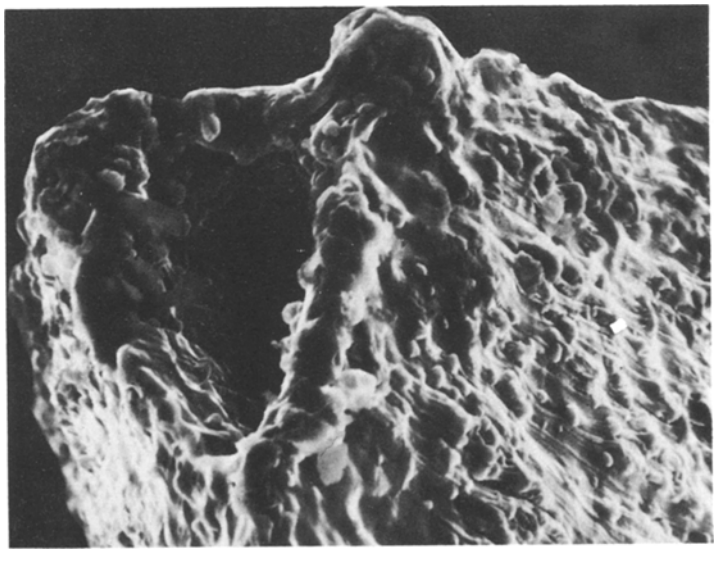

Figure 14. Scanning electron micrograph showing the cavitation at the tip fracture in an Al–Ca alloy specimen tested at an initial strain rate of $4.16 \times 10^{-2}\,sec^{-1}$ (region III). The corrugated external surface of the samples is also visible (× 700).

istic of the superplastic alloys which cavitate extensively such as the Al–Pd [22] eutectic. In the case of the present alloy the failure behaviour can be classified following the experimental results of the former type. In practice several necks grow slowly simultaneously (instability I) before the growth of one of these necks predominates and becomes rapid and catastrophic (instability II). The latter and final stages of cavitation are closely related and the microstructural feature (Figs. 12 and 13) agrees well with the model of Taplin *et al.* [24]: the ligaments between the cavities are themselves resistant to internal necking and to micro-intrinsic plastic failure and the final catastrophic coalescence is due to the void linkage of internal ligaments. Nevertheless, the ligament strain rate would be so rapid that it is difficult to explain the high strain rate sensitivity shown by the intercavity material. However, there is mictrostructural evidence (Figs. 12 and 13) that ligaments are constituted not by pure aluminium but by a two phase material (aluminium plus a high density of very fine Al–Ca particles not separated by the matrix during deformation). This suggests a rate sensitivity flow of the intercavity material justified by a fine scale (stable) subgrain network due to the high density of the second phase particles.

3.6. Deformation mechanisms

The results obtained are not sufficiently convincing to identify a rate controlling deformation mechanism, because they cover only one temperature (773 K) and one grain size ($L \sim 3\,\mu m$). Moreover, there is a scarcity of data concerning the diffusivity and the activation energy for grain boundary diffusion in aluminium, and for interdiffusion on Al_4Ca*. However, although a quantitative verification of a theory is rather difficult or impossible, it would be interesting to examine the theories which account for the principal features in the above sections.

The features of region II of superplasticity which deserve more attention are:

(a) the stress–strain rate behaviour is a straight line (slope $m = 0.32$) and there is no evidence of a conventional region I;

(b) there is no evidence of a threshold stress;

(c) no large grain elongation; extensive grain boundary sliding and a significant dislocation pile-ups within the grains. The dislocation activity varies from grain to grain;

(d) the equiaxed grain is maintained after a strain of one hundred per cent;

(e) grain growth occurs concurrently during superplastic deformation.

These phenomenological and microstructural features are all accounted for by the theories based on the accommodation of grain boundary sliding (dominant microscopic process) and by intragranular slip involving dislocation pile-ups. These models are due to Ball and Hutchinson [25] and Mukherjee [26], and are fairly similar. In the former the grains slide in groups whereas in the latter the grains slide individually. The two theories [25, 26] also state that superplasticity is a unique mechanism and predict a linear $\log\sigma$–$\log\dot{\epsilon}$ relationship, and no occurrence of the region I and of a threshold stress. The explanation of the superplastic deformation behaviour by a model combining grain boundary sliding and dislocation motion within the grains was proposed previously for other Al-based systems, Al–Cu and Al–Mg superplastic alloys by Matsuki *et al.* [27, 28]. Recent critical reviews [29, 30] stress the importance of dislocation accommodation mechanisms in describing the superplasticity.

4. Conclusions

1. It is confirmed that the hot rolled Al–Ca eutectic alloy exhibits a superplastic behaviour manifested by a very high elongation ($> 300\%$) and a high strain rate sensitivity ($m > 0.30$) when deformed at high temperature ($T = 773$ K).

2. An apparent sigmoidal shape of the $\log\sigma$–$\log\dot{\epsilon}$ curve in region I was observed at low strains due to the grain growth and the variation of m with strain at low strain.

3. At higher strains ($\epsilon \cong 0.7$) where the stress is not sensitive the $\log\sigma$–$\log\dot{\epsilon}$ curve becomes a straight line. Two regions are delineated: a superplastic region II ($2 \times 10^{-5} \leqslant \dot{\epsilon} \leqslant 4 \times 10^{-2}\,sec^{-1}$) ($m = 0.32$) and a dislocation creep regime region III ($\dot{\epsilon} > 4 \times 10^{-2}\,sec^{-1}$) ($m = 0.13$).

4. There was evidence that the dislocation interacts with very fine particles and precipitates within the aluminium matrix grains in the specimens deformed in region II.

5. The superplastic flow process can be qualitat-

*According to [6] the diffusion coefficient of calcium in aluminium is expected to be low because of the low solubility of calcium in aluminium and the high atomic radius of calcium 0.197 nm, compared to 0.143 nm for aluminium.

ively explained by the assumption of grain boundary sliding accommodated by dislocation motion within the aluminium matrix grains.

6. The alloy specimen deformed in the superplastic region pulls down to a very fine point of fracture with a reduction area near to 100%. However, the final fracture depends on a void linkage mechanism which includes on a microscopical scale the internal necking of the tiny ligaments between the cavities.

Acknowledgements

Discussions with Dr P. Schiller are acknowledged with pleasure. Technical assistance was given by Miss T. Stoto, Mrs M. Romor and D. Boerman, R. Baranzini, E. Haine, F. Quazzo and H. P. Weir. Thanks are also due to Dr R. Grimes (British Aluminium Company Ltd) for helpful comments during the preparation of the manuscript, to Mrs L. Ottolini (ISML-Alluminio Italia) for TEM analysis and to Mrs E. Staroste (formerly Ispra) for SEM analysis.

References

1. G. PIATTI, G. PELLEGRINI and R. TRIPPODO, Proceedings of the 6th International Conference on Light Metals, Leoben, Vienna, 1975 (Aluminium Verlag. Düsseldorf, 1976) p. 45.
2. *Idem, J. Mater. Sci.* **11** (1976) 186.
3. R. GRIMES, A. J. CORNISH and R. G. BUTLER, Proceedings of the 7th International Conference on Light Metals, Loeben, Vienna, 1981 (Aluminium Verlag, Düsseldorf, 1982) p. 302.
4. R. GRIMES, "Shaping Metals for the Eighties" (Metallurgical Society Meeting, London, 1981).
5. R. MATERA, G. PIATTI and K. N. STREET, *Aluminium* **49** (1973) 335.
6. J. C. JAQUET and H. WARLIMONT, *Z. Metalkd.* **72** (1981) 13.
7. L. PERALDO-BICELLI, G. ROMAGNANI and D. SINIGAGLIA, *Corros. Sci.* **19** (1979) 553.
8. L. F. MONDOLFO, "Aluminium Alloys: Structure and Properties" (Butterworths, London, 1976) p. 238.
9. G. PELLEGRINI and G. PIATTI, *Mater. Sci. Eng.* **34** (1978) 171.
10. K. N. STREET, F. C. St. JOHN and G. PIATTI, *J. Inst. Met.* **95** (1967) 326.
11. D. W. LIVESEY and N. RIDLEY, *J. Mater. Sci.* **13** (1978) 825.
12. B. M. WATTS and M. J. STOWELL, *ibid.* **6** (1971) 228.
13. M. SUERY and B. BAUDELET, "Creep of Engineering Materials and Structures", edited by G.Bernasconi and G. Piatti (Applied Science Ltd, London, 1979) p. 47.
14. J. W. EDINGTON, K. N. MELTON and C. P. CUTLER, *Progr. Mater. Sci.* **21** (1976) 61.
15. K. A. PADMANABHAN and G. J. DAVIES, "Superplasticity" (Springer-Verlag, Berlin, 1980).
16. B. P. KASHYAP and G. S. MURTY, *Mater. Sci. Eng.* **50** (1981) 205.
17. R. J. LEDERICH, S. M. L. SASTRY, M. HAYASE and T. L. MACKAY, *J. Met.* **34** (1982) 16.
18. G. RAI and N. J. GRANT, *Met. Trans.* **6A** (1975) 385.
19. S. T. LAM, A. ARIELI and A. K. MUKHERJEE, *Mater. Sci. Eng.* **40** (1979) 73.
20. D. A WOODFORD, *Trans, ASM* **62** (1969) 291.
21. A. K. GHOSH and R. RAJ, *Acta Metall.* **29** (1981) 607.
22. G. PIATTI and M. BARDY, *Met. Sci.* February (1981) 55.
23. D. A. MILLER and T. G. LANGDON, *Metall. Trans.* **9A** (1978) 1688.
24. D. M. R. TAPLIN, G. L. DUNLOP and T. G. LANGDON, *Ann. Rev. Mater.* **9** (1979) 151.
25. A. BALL and M. M. HUTCHINSON, *Met. Sci. J.* **3** (1979) 1.
26. A. K. MUKHERJEE, *Mater. Sci. Eng.* **8** (1971) 83.
27. K. MATSUKI, Y. UETAMI, M. YAMADA and Y. MURAKAMI, *Met. Sci.* **10** (1976) 235.
28. K. MATSUKI, K. MINAMI, M. TOKIZAWA and Y. MURAKAMI, *ibid.* **13** (1979) 619.
29. T. G. LANGDON, *Met. Trans.* **13A** (1982) 689.
30. A. ARIELI and A. K. MUKHERJEE, *ibid.* **13A** (1982) 717.

Received 29 December 1982
and accepted 20 January 1983